

Article

A Joint Design of Radar Sensing, Wireless Power Transfer, and Communication Based on Reconfigurable Software Defined Radio

Zhouyi Wu ^{1,2}, Yasser Qaragoz ¹, Vladimir Volskiy ¹, Jiangtao Huangfu ², Lixin Ran ² and Dominique Schreurs ^{1,*} ¹ Division ESAT-WaveCoRE, KU Leuven, 3000 Leuven, Belgium² Laboratory of Applied Research on Electromagnetics (ARE), Zhejiang University, Hangzhou 310027, China

* Correspondence: dominique.schreurs@kuleuven.be; Tel.: +32-16-321821

Abstract: This paper proposes a compact three-mode base station capable of performing radar sensing, communication, and wireless power transfer (WPT) in collaboration with indoor sensor networks. With regard to the wireless sensor node, the base station transmits two-tone signals in the downlink to support its operation and provides two-way communication. The sensor node sends uplink information through backscattering using the third order intermodulation (IM3) product of the rectification. In the radar mode, a single-tone continuous wave (CW) is used to monitor if there is a moving target in the static environment. If a speed is detected, the transmit signal to the node is stopped, while the single-tone CW excitation will continue until the speed of the target is zero, and then the base station transmits a stepped frequency continuous wave (SFCW) signal to measure the distance of the target. The repeat between the two radar waveforms continues until the target is undetectable within the detection range. The software defined radio PlutoSDR is adopted as the base station. The system can wirelessly supply power and bi-directionally communicate with a CO₂ sensor node 2 m away. It gives a range resolution of 2.5 cm and a minimum detectable speed of 0.25 m/s in the radar mode.

Keywords: communication; radar; SFCW; software defined radio (SDR); wireless power transfer (WPT)



Citation: Wu, Z.; Qaragoz, Y.; Volskiy, V.; Huangfu, J.; Ran, L.; Schreurs, D. A Joint Design of Radar Sensing, Wireless Power Transfer, and Communication Based on Reconfigurable Software Defined Radio. *Electronics* **2022**, *11*, 4050. <https://doi.org/10.3390/electronics11234050>

Academic Editor: Dimitra I. Kaklamani

Received: 2 November 2022

Accepted: 3 December 2022

Published: 6 December 2022

Publisher's Note: MDPI stays neutral with regard to jurisdictional claims in published maps and institutional affiliations.



Copyright: © 2022 by the authors. Licensee MDPI, Basel, Switzerland. This article is an open access article distributed under the terms and conditions of the Creative Commons Attribution (CC BY) license (<https://creativecommons.org/licenses/by/4.0/>).

1. Introduction

Millions of Internet of Things (IoT) nodes have been employed during the past decades [1,2]. In view of the emerging intelligent industry and living, the number of sensor nodes will continue to increase as sensing is the basis of intelligence. These nodes monitor devices and the environment, communicate with base stations, and need a power supply to support their operation, all of which create challenges for the management of the overall network [3,4]. In order to control system redundancy and reduce network complexity, studies have been carried out to integrate several techniques, such as unifying microwave power transfer and wireless communications. One of the strategies is to send power in the downlink from a base station or a power beacon to the sensor node, and transfer information in the uplink using the received power [5,6]. In [7], the power signal from the base station is at 5.5 GHz, and the information transfer function works at 3.5 GHz. Similar dual-frequency information and power transfer solutions also appear in [8,9].

Another kind of work is simultaneous wireless information and power transfer (SWIPT) [10,11], which simultaneously sends power and information in the downlink from the base station. High isolation between information and energy flows is usually required for such system designs [12]. Ref. [13] proposes a tunable dual-port 5.8 GHz system for both energy harvesting and Wi-Fi data streaming. These two modes can be performed independently, or the harvested energy from one port can be used for communication on the other port. In addition, research on spatial modulation [14] and time division [15] methods are also reported to achieve separate processing of the information

and power signals at the receiver side. These works eliminate most cables in the sensor network. The capacity of energy storage elements can also be reduced on the node, if the wireless power from the base station can meet the needs of the node's operation. Further, ref. [16] proposes a system that integrates spectrum sensing, wireless power transfer (WPT), and communication simultaneously. The added spectrum sensing function helps to sense idle channels and achieve flexible spectrum access for data transmission.

When it comes to indoor sensor networks, the interaction between the radiating system and the human body must be considered. If the power required to support the operation of the sensors is entirely provided by wireless transfer, human detection in a sensor network-distributed room becomes indispensable in order to avoid possible exposure to radiation. Compared to adding another sensor, developing sensing function in the SWIPT system is obviously a better choice [17]. Since communication systems are often developed according to the requirements of communication and strict standards of modulation bandwidth, the main stream radar waveforms with a wide bandwidth are inoperative. Therefore, a study on integrating radar functionality in the original communication and power transfer system is necessary.

Digitalized wireless platforms realize various transmitting and receiving functions by way of upgradable and reconfigurable software [18]. Most of the signal processing is handed over to computers or embedded systems, which releases the burden of hardware design and makes it easier to configure a transceiver. Software defined radio (SDR) is one of the development tools. As a highly versatile communication system, SDR has been used to serve as an RFID reader [19], non-contact measurement tool [20], interrogator of sensor networks [21], radar receiver [22], and is also used in medical imaging systems [23]. Two typical fields of its application are cognitive radio and vehicular networking [24]. In cognitive radio, combined with machine learning techniques, SDR is able to perform environment sensing, adapt operating behaviors, and learn from new situations. Further, SDR is adopted as the physical layer of vehicular networking to realize the updating of network topology [25]. Therefore, the application of SDRs in more systems can be expected.

In this paper, a joint design of radar sensing, WPT, and communication is proposed based on SDR to make a compact three-mode system that contains a base station and the sensor node. The base station simultaneously transfers power and information to the sensor node using a two-tone signal, and also sends radar waves for human detection in the room. The sensor node harvests energy and transfers information back through backscattering. This is the first time that WPT, communication, and radar sensing have been integrated. The approach provides a solution for adding radar functionality to existing communication systems with a reduced impact on their original architecture and collaborative relationship. The system design is presented in Section 2. Signal formulations of the three modes are analyzed in Section 3. Experimental investigations are carried out in Section 4. Section 5 presents a conclusion.

2. System Design

An SDR is adopted in this work as the base station to realize the three modes. As illustrated in Figure 1, the base station transfers power in the downlink, and provides two-way communication for the sensor node. The sensor node consists of an energy-harvesting node and a sensor. Moreover, radar signals are transmitted to detect the speed and distance of the human target.

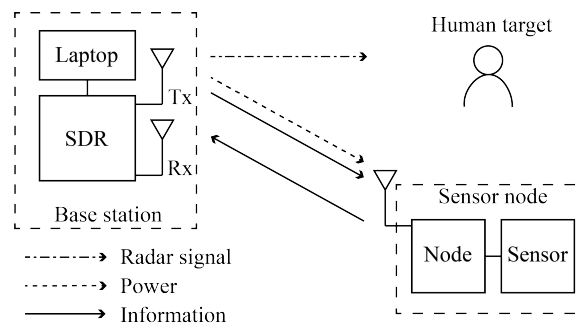


Figure 1. Top-level representation of the proposed three-mode system.

The existing indoor human detection radar mainly works in ISM bands such as 2.4 GHz, 24 GHz, and 60 GHz. There are two kinds of radar waveforms, pulse and continuous wave (CW). Research on pulse radar focuses on the ultra-wideband (UWB) pulse. The UWB bandwidth should exceed the minimum of 500 MHz or 20% of the amount of the center frequency. Single-tone CW can only measure the speed of moving targets, while frequency-modulated continuous wave (FMCW) is the main-stream continuous waveform that can simultaneously measure the speed and range of the target. An FMCW system transmits chirp signals whose frequency varies linearly with time, and calculates the target distance from the down converted received signals. The range resolution ΔD depends on the bandwidth of the chirp, and can be calculated as:

$$\Delta D = \frac{c}{2B}, \quad (1)$$

where c is the speed of light and B is the bandwidth. As a narrower bandwidth leads to a lower range resolution, an FMCW radar usually has a bandwidth of 1–4 GHz in order to detect human targets [26,27]. By contrast, the performance of SDRs follows the requirements of a communication system, which has limited modulation bandwidth under strict standards. Most commercial SDRs have an RF bandwidth in the range of about 20–60 MHz, along with a frequency range under 6 GHz. Therefore, the above types of radar will produce compromised quality in terms of range resolution if they are realized on an SDR platform.

Different from these wideband waveforms, the stepped frequency continuous wave (SFCW) waveform sweeps through a bandwidth at discrete frequency values with a fixed step. The instantaneous bandwidth at every step is narrow, but when combined together, the effective bandwidth is large. Since SDR systems have a wide tunable range of center frequency and a relatively low modulation bandwidth, they are able to obtain a range resolution as high as main stream wideband radars by sweeping the carrier frequency. Compared to FMCW, which occupies the whole frequency band, SFCW only uses a narrow band at every frequency step. The idle frequencies in the spectrum can be utilized for coordination among the nodes of the network, which helps to reduce the impact brought about by incorporating radar functionality into the communication system [28]. Meanwhile, a lower bandwidth of the receiver leads to receiving signals with less noise. Considering that the high sensitivity of the receiver is an advantage of the communication system, combining SFCW with SDR will present a satisfactory sensitivity and anti-interference performance.

However, it usually takes some time for the SDR to change the center frequency of the transmitting signal, which makes it time-consuming for the SFCW method to complete a measurement. To promptly obtain the state of the environment, a single-tone CW is required to check for moving objects instead. In this paper, a time splitting strategy is adopted to arrange the operation of three modes.

The power and information transfer are performed between the base station and the sensor node. A two-tone signal is adopted as the SWIPT waveform at the base station in the downlink. During the node rectification process, the harvested energy serves as the power supply, and the generated third order intermodulation (IM3) products are used

as the carrier of the uplink. Data obtained from the sensor are modulated onto the IM3 products, and are then sent to the base station.

As illustrated in cycle 1 in Figure 2, after some time interacting with the node, the base station switches to transmit single-tone CW to check whether there is a speed change in the environment. If no speed information is recovered from the reflected radar signals, the base station continues to send waveforms for SWIPT. Otherwise, cycle 1 is stopped and the base station switches to the radar mode cycle 2 on the right. The CW waveform continues. After the measured speed returns to zero, the base station sends the SFCW waveform to measure the distance between the target and the base station. The radar mode will repeat between CW and SFCW until both the speed and distance of the human target become undetectable within the detection area. Then, the base station resumes to the cycle of SWIPT, communication, and CW radar.

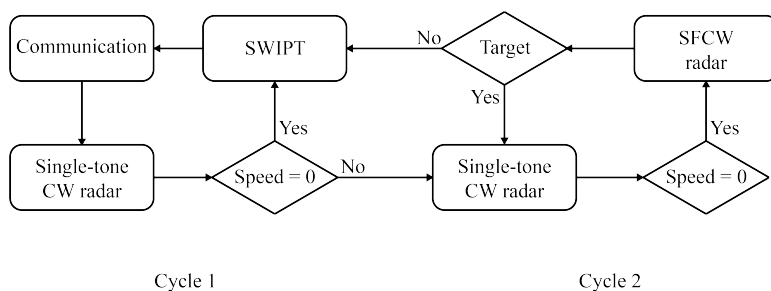


Figure 2. Assignment of three modes at the base station.

3. Signal Formulations

In the process of three-mode operation, the base station outputs three kinds of waveforms, including a two-tone signal, a CW signal, and an SFCW signal. As this method is adapted to SDR, the phase introduced by the transceiver chain is also analyzed.

3.1. Wireless Power Transfer and Communication

A closely-spaced two-tone signal is used at the base station to simultaneously transfer power and information to the sensor node, whose time-domain waveform can be expressed as:

$$V_{tx} = A_0 \cos(\omega_1 t) + (1 - A_0) \cos(\omega_2 t), \tag{2}$$

where ω_1 and ω_2 are frequencies of the two tones with $\omega_2 > \omega_1$, and A_0 is the ratio of their amplitudes with a range from 0 to 1. The path loss from base station Tx antenna to the node rectenna is G . The DC component produced by rectification is used to supply power to the node, while the IM3 products generated by the nonlinearity of the rectifier circuit at frequencies $2f_1 - f_2$ and $2f_2 - f_1$ are used for backscatter communication. The magnitudes of the excited upper and lower IM3 current at the input of rectifier can be expressed as [29]:

$$I_{lower} = G^3 b A_0^2 (1 - A_0), \tag{3}$$

$$I_{upper} = G^3 b (1 - A_0)^2 A_0, \tag{4}$$

where b is a real number coefficient. The IM3 at upper frequency $2f_2 - f_1$ is adopted as the carrier to modulate the baseband data stream from the sensor, and then the modulated signal is transmitted back to the base station.

3.2. Single-Tone CW Radar

For a CW radar, the Doppler shift f_d caused by a moving object follows the equation below [30]:

$$f_d = \frac{2}{\lambda} v_r, \tag{5}$$

where λ is the wavelength, v_r is radial speed of the target with respect to the base station. For objects moving at the same velocity, a CW with a smaller wavelength produces a larger Doppler frequency shift.

3.3. SFCW Radar

The SFCW radar transmits sequences of continuous wave at designed frequency steps. The transmitted signals can be expressed as:

$$s_k(f_k, t) = \cos(2\pi f_k t + \varphi_k(t)), \quad (6)$$

where $f_k = f_0 + k\Delta f$, f_0 is the starting frequency, Δf is the frequency step, k is the number of frequency steps, and $\varphi_k(t)$ is the initial phase of the k -th transmitted signal. When the transmitter and receiver of the radar are placed close to each other, the received echo signal $r_k(f_k, t)$ from a stationary target at distance D can be calculated as:

$$r_k(f_k, t) = \cos\left(2\pi f_k \left(t - \frac{2D}{c}\right) + \varphi_k\left(t - \frac{2D}{c}\right)\right). \quad (7)$$

After the quadrature detection of the receiver, the received echoes are down-converted to in-phase (I) and quadrature (Q) baseband signals by mixing with a copy of the corresponding transmitted waveforms. The complex output signal can be expressed as [31]:

$$u_k(f_k) = I_k(f_k) + jQ_k(f_k) = \exp\left(-j\left(2\pi f_k \frac{2D}{c} + \theta_k\right)\right). \quad (8)$$

θ_k includes the phase shift introduced by the target surface and the mixer, which is a fixed value and can be compensated through calibration. The inverse discrete Fourier transform (IDFT) is used to recover the range profile of the target from the output signal as:

$$S_n = \frac{1}{N} \sum_{k=0}^{N-1} \exp\left(j\frac{2\pi nk}{N} - j\frac{4\pi f_k D}{c}\right), \quad (9)$$

where N is the number of frequency steps. This equation can be solved as [32]:

$$S_n = \frac{1}{N} \exp\left(-j\frac{4\pi D f_1}{c}\right) \frac{\sin(aN/2)}{\sin(a/2)}, \quad (10)$$

where $f_1 = f_0 + \frac{N-1}{2}\Delta f$, and $a = \frac{2\pi}{N}\left(n - \frac{2DN\Delta f}{c}\right)$. Therefore, the magnitude response of the IDFT is as follows:

$$|S_n| = \frac{1}{N} \left| \frac{\sin(aN/2)}{\sin(a/2)} \right|. \quad (11)$$

It is a synthetic pulse consisting of N lobes. The lobe peak locates at number n_p where $a = 0$. The target distance D in terms of n_p falls at:

$$D = \frac{cn_p}{2N\Delta f}. \quad (12)$$

3.4. Mixer-Introduced Phase

The phase of the output signal after mixing is subject to the time when the signal enters the mixer. If the transceiver has one mixer, the transmitting and receiving signals follow the same time sequence. If the transmit and receive chains have separate mixers, signals from the Tx local oscillator (LO) mix with the generated baseband signal, while signals from the Rx LO mix with the received signals. If the two mixers are time-synchronized, the phase introduced by mixing will be controllable. However, in some SDRs, separate mixers are used for transmitting and receiving chains without time synchronization. In this

case, the expression of transmitted signals in (6) and the complex output after quadrature detection in (8) can be modified as:

$$s_k(f_k, t) = \cos(2\pi f_k t + \varphi_k(t) + \varphi_{tx}), \quad (13)$$

$$u_k(f_k) = \exp\left(-j\left(2\pi f_k \frac{2D}{c} + \theta_k + \varphi_{tx} - \varphi_{rx}\right)\right), \quad (14)$$

where φ_{tx} and φ_{rx} represent the phases introduced by the Tx and Rx mixers, respectively. The phase of the mixed signal varies every time the mixers are powered up or the LO frequency is changed. In the next section, a solution is discussed to alleviate this problem.

4. Experimental Investigations

4.1. Reference Path and Measurement Path

As shown in Figure 3, a commercial SDR, ADALM-PLUTO SDR Active Learning Module (PlutoSDR), is adopted as the base station. The internal transceiver IC AD9363 has two separate LOs without time synchronization. Therefore, the additional phase term $\varphi_{tx} - \varphi_{rx}$ in (14) is random and different for every frequency step, depending on the performance of the two LOs. To eliminate the random phase, a reference path is introduced in Figure 3. The Tx port of PlutoSDR is connected to the input port of a HMC641ALC4 RF switch module, and the Rx port is connected to a ZFRSC-123-S+ power combiner. A short coaxial cable is connected from the RF3 port of the RF switch to the port 1 of power combiner via a 20 dB attenuator to form the reference path of signal. The Tx and Rx antennas are respectively connected to the RF1 port of the RF switch and port 2 of the power combiner to form the measurement path. At every frequency step of SFCW, the RF switch is switched to the RF3 port first, and then to the RF1 port while keeping the state of the transmitting chain unchanged. Signals from the reference path and measurement path pass through the power combiner in turn to the receiver. Since the Tx and Rx LOs are unchanged in this process, the term $\varphi_{tx} - \varphi_{rx}$ is identical for the reference path and the measurement path. This extra random phase caused by the asynchronization between two chains can be eliminated by subtracting the phase of the reference path from that of the measurement path.

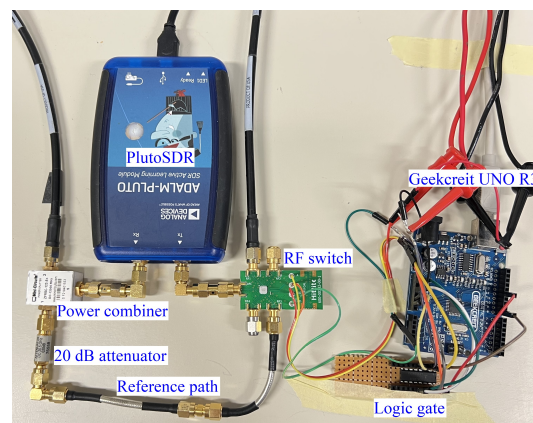


Figure 3. Structure of the reference path and measurement path.

PlutoSDR has one transmitter and one receiver, with an RF coverage from 325 MHz to 6 GHz. The RF switch is controlled by a Geekcreit UNO R3 board via a DG412DJZ logic gate. Except for working in SFCW of the radar mode, the RF switch is always connected to port RF1 in the measurement path when the system is in SWIPT, communication, and CW radar modes.

4.2. SFCW Ranging

The overall experimental system is shown in Figure 4a. Two GH1-18N horn antennas working at 1–18 GHz are used as the Tx and Rx antennas. The transmitting signal is amplified by a power amplifier before entering the Tx antenna, which enables the base station to provide sufficient power to the sensor node 200 cm away. The frequency range of the SFCW radar mode is 1–3 GHz, with a frequency step of 25 MHz. The carton with the metal plate is moved from 12.5 cm to 200 cm in front of the antennas. A distance list of 200 cm, 170 cm, 140 cm, 110 cm, 80 cm, 50 cm, and 20 cm is set with a 30 cm difference. Around distances of 170 cm, 140 cm, 110 cm, 80 cm, 50 cm, and 20 cm, seven points including the original distance, distances ± 2.5 cm, ± 5 cm, and ± 7.5 cm away are measured. For the distance of 200 cm, four points at 200 cm, 200–2.5 cm, 200–5 cm, and 200–7.5 cm are measured. Therefore, there are 46 points in total within the range of 200 cm. Figure 4b shows the results of SFCW ranging after calibration. The horizontal axis is the actual distance of the object. The vertical axis is the measured distance. The measurement error is less than 0.65 cm when the distance is more than 1 m, while within 1 m, the error tends to gradually increase as the distance from the object to the antennas decreases. When the distance is 15 cm, the error reaches a maximum of 11.25 cm. In the frequency range of the SFCW radar mode, as the object comes closer to the antennas within 1 m, it gradually leaves the far-field region. However, even if there is a deviation in the measured distance, the presence of the object near the antenna can still be detected, which will not cause misjudgment in the operation of cycle 2. It takes 0.9 s to measure a frequency step, including time to alter the carrier frequency of PlutoSDR, to change ports of the RF switch, and the time to perform the actual measurement. An 81-frequency SFCW requires 72.9 s to measure the distance, and 0.5 s for data processing.

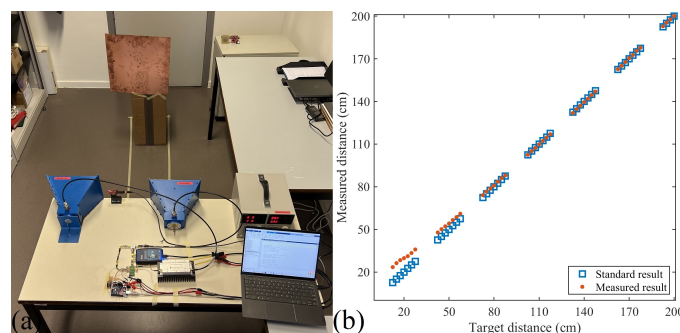


Figure 4. (a) Experimental setup for SFCW range test. (b) Result of SFCW radar ranging.

In the test field, there is no obstruction from the front of the antenna to the door of the room. Therefore, the distance where the highest peak of the reflected power distribution is located is the distance between the target and the antenna. For furnished rooms, an additional calibration step has to be added, namely the room needs to be measured when no one is present. In that case, the distribution of reflected power is recorded as the calibration data that should be subtracted from the power distribution result in the presence of a target during data processing.

4.3. CW Speed Validation

The frequency of CW radar is set to the highest frequency of 6 GHz that the PlutoSDR can provide. As shown in the enlarged area of Figure 5a, an IWR6843 antenna-on-package (AoP) radar module from Texas Instruments (TI) is adopted as a reference for speed measurement, and is placed next to the Tx horn antenna. Since this module works at 60 GHz, there is no interference between the two radars. The measured speed of a person walking back and forth in front of the horn antennas is presented in Figure 5b. The PlutoSDR in radar mode provides a minimum detectable speed of 0.25 m/s.

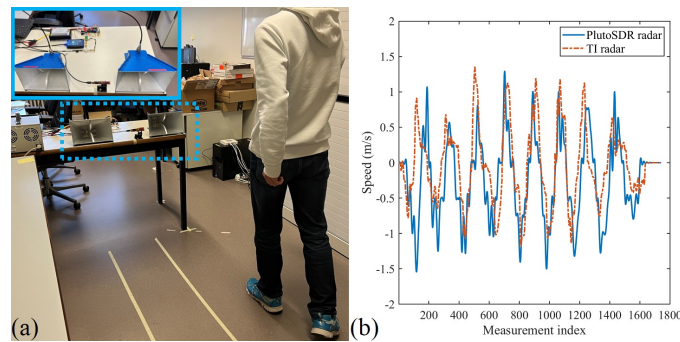


Figure 5. (a) Experimental setup for CW speed test. (b) Speed measurement results of PlutoSDR radar and TI radar.

4.4. SWIPT and Node Communication

Wireless power transfer and communication involve the base station and the sensor node. In this system, the PlutoSDR transfers power and information simultaneously to the sensor node in the downlink. The node receives power and sends back information in the uplink through backscattering. The downlink two-tone signal is generated using differential frequency shift keying (DFSK) at 2.538 GHz, with modulation frequencies of 100 kHz and 300 kHz. The node backscatter is at 2.5385 GHz, and amplitude shift keying (ASK) modulation is used. As shown in Figure 6, the sensor node consists of a rectification and backscatter node, a CozIR-LP CO₂ sensor, a MSP430FR5994 LaunchPad Development Kit microcontroller unit (MCU), and a patch antenna. During the bi-directional communication, the base station sends information in the downlink, including a 3-byte preamble, a 2-byte nonce, and the ID of the sensor node. After passing the verification, the sensor node replies repeatedly with a message consisting of 3-byte preamble, the same ID and nonce, the 2-byte CO₂ sensor readout, and two 13-byte fixed values as padding. As illustrated in Figure 7, there are 35 bytes in a message from the sensor node.

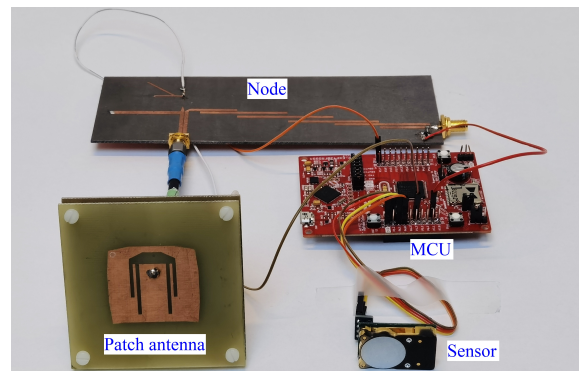


Figure 6. Structure of the sensor node.

Preamble	ID	Nonce	Sensor result	Fixed padding 1	Fixed padding 2
3 bytes	2 bytes	2 bytes	2 bytes	13 bytes	13 bytes

Figure 7. Components of the uplink information.

A typical usage of the sensor is to take a reading every minute. Therefore, the period of cycle 1 in Figure 2 is set to 60 s, of which SWIPT lasts for the first 55 s. The rectified DC component charges a 1 F supercapacitor that acts as the power source of the MCU. The MCU reads data from the sensor once per cycle. From 50 to 55 s, the node demodulates instructions from the DFSK waveform and modulates information in the ASK waveform. Only in the presence of two-tone input can the data be modulated onto the IM3 carrier and reflected back to the base station. Then, CW radar mode is performed in the last 5 s of cycle

1. If this cycle is paused and the base station turns to cycle 2 in Figure 2, the two-tone input at the node and the accompanying IM3 products for uplink modulation will be suspended as well.

The DFSK demodulation consumes $728 \mu\text{W}$ in 0.7 s per cycle. The CozIR-LP CO_2 sensor requires $417 \mu\text{W}$ to take a reading every minute under default settings. The uplink transmission process repeats the message 16 times, and a total of 4480 bits are sent in a period of 2 s. The two padding sequences with fixed values can be used for additional functions such as encryption keys. An average power of $264 \mu\text{W}$ is consumed at the MCU for ASK modulation. The sensor node is placed 2 m away from the base station. The tag is presented in the previous work [33], which has an average harvested power of $32.75 \mu\text{W}$ when -10 dBm power is provided at the rectifier circuit. The measured maximum output power of PlutoSDR around 2.538 GHz is 3 dBm. In view of the 46 dB free-space path loss during propagation, a 23 dB power amplifier is connected between the Tx antenna and the RF1 port of the RF switch at the base station. The receive gain of PlutoSDR is set to a high level to obtain uplink information. Correspondingly, in order to prevent saturation of the input signal at receiver chain in the SFCW radar mode, the 20 dB attenuator is added in the reference path.

4.5. Time Sequence of the Three Modes

This system arranges the three modes by time splitting. First, the base station sends 55 s of SWIPT waveform to power the node and provides the IM3 component required by uplink backscattering. Starting from the 50th second, the node demodulates the downlink signal to acquire instructions for sensor access. Then, the data from the CO_2 sensor are modulated onto the IM3 product in ASK modulation, and are repeatedly sent to the base station within a period of 2 s. Correspondingly, the base station receives and demodulates the signal for 5 s, followed by 5 s of speed detection in CW radar mode. This 60-s process is illustrated in cycle 1 in Figure 8. If no speed is detected from the current scene, cycle 1 continues. Otherwise, the base station turns to cycle 2 while maintaining the CW radar mode until the calculated speed returns to 0. Then, the succeeding SFCW radar mode measures the distance of the target. It takes 73.4 s to finish 81 frequency steps and the data processing. This is illustrated in cycle 2 in Figure 8. If no target is detected within the detection range, the base station resumes to cycle 1. If the target remains in the scene, cycle 2 will repeat.

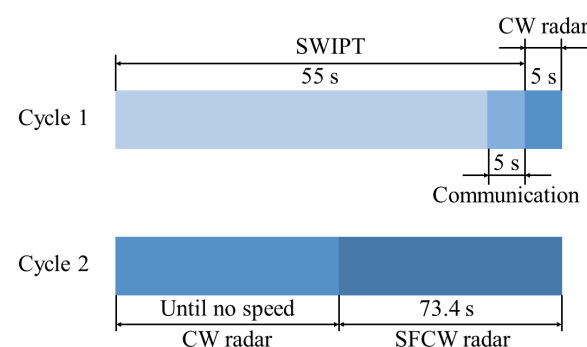


Figure 8. The time allocated for each mode in the two cycles.

In situations where the power transmitted to the sensor is higher, more frequent insertion of the CW mode during the SWIPT process can be adopted, such as speed monitoring every 30 s. This leads to a smaller window of time during which a person is likely to be exposed to radiation. Further, the measuring time of the target range in SFCW radar mode is a result of the trade-off with the range resolution. A higher number of frequency steps means denser sampling over the spectrum. Reducing the number of steps can shorten the measuring time. However, the range will be accordingly divided into sparser cells, which leads to a reduced resolution.

5. Conclusions

The joint design of radar sensing, WPT, and communication is proposed in this paper. Based on a reconfigurable SDR, the base station is capable of powering and communicating with the nodes of an indoor wireless sensor network by SWIPT waveform and backscattering, and detecting the presence of a human through radar sensing. The energy harvested from the SWIPT waveform is accumulated in the sensor node as the power source. The three modes of the base station are achieved by time splitting strategy. During the 60-s cycle 1, the base station sends two-tone signals to simultaneously transfer power and information to the sensor node, and then receives information from the node through backscattering. The speed detection is executed at the end of every cycle to check the potential presence of a human object. When a moving object is detected, the power and information signals are halted, while the speed and distance measurements will continue until the moving object leaves the area. The minimum detectable speed is 0.25 m/s. A range resolution of 2.5 cm is achieved by means of SFCW on the PlutoSDR. A trade-off between measurement time and range resolution is essential when implementing radar function on communication platforms. This system is suitable for indoor environments where wireless sensor nodes are distributed and humans may appear, such as in hospitals, smart homes, and industrial plants. In future work, a multiple-input and multiple-output (MIMO) antenna array can be introduced to calculate the distance and orientation of the targets to achieve indoor localization.

Author Contributions: The idea was proposed by D.S. and L.R.; the theoretical analysis of the method and the experimental investigations were performed by Z.W.; Y.Q. contributed to the sensor node part; V.V. provided support for the experiments; J.H., L.R. and D.S. supervised this work. All authors participated in the revision of the manuscript. All authors have read and agreed to the published version of the manuscript.

Funding: This work was supported by the National Natural Science Foundation of China (NSFC) under Grant 62111530096, and the Research Foundation—Flanders (FWO) of Belgium under Grant VS02321N and G085818N.

Data Availability Statement: The data produced and the developed codes of the current study are available from the corresponding author on reasonable request.

Conflicts of Interest: The authors declare there are no conflicts of interest regarding the publication of this paper.

References

1. Zeadally, S.; Shaikh, F.K.; Talpur, A.; Sheng, Q.Z. Design architectures for energy harvesting in the Internet of Things. *Renew. Sustain. Energy Rev.* **2020**, *128*. [[CrossRef](#)]
2. Huda, S.M.A.; Arafat, M.Y.; Moh, S. Wireless power transfer in wirelessly powered sensor networks: A review of recent progress. *Sensors* **2022**, *22*, 2952. [[CrossRef](#)] [[PubMed](#)]
3. Chiu, C.C.; Chien, W.; Chen, P.H.; Cheng, Y.T.; Jiang, H.; Chen, E.L. Optimization for an indoor 6G simultaneous wireless information and power transfer system. *Symmetry* **2022**, *14*, 1268. [[CrossRef](#)]
4. Ashraf, N.; Sheikh, S.A.; Khan, S.A.; Shayea, I.; Jalal, M. Simultaneous wireless information and power transfer with cooperative relaying for next-generation wireless networks: A review. *IEEE Access* **2021**, *9*, 71482–71504. [[CrossRef](#)]
5. Zhou, S.; Wang, X.; Cao, N.; Li, X. Performance analysis of wireless powered communications with multiple antennas. *IEEE Access* **2018**, *6*, 15541–15549. [[CrossRef](#)]
6. Han, K.; Huang, K. Wirelessly powered backscatter communication networks: Modeling coverage and capacity. *IEEE Trans. Wirel. Commun.* **2017**, *16*, 2548–2561. [[CrossRef](#)]
7. Zhang, J.; Meng, J.; Li, W.; Yan, S.; Vandebosch, G.A.E. A wearable button antenna sensor for dual-mode wireless information and power transfer. *Sensors* **2021**, *21*, 5678. [[CrossRef](#)]
8. Wagih, M.; Hilton, G.S.; Weddell, A.S.; Beeby, S. Dual-band dual-mode textile antenna/rectenna for simultaneous wireless information and power transfer (SWIPT). *IEEE Trans. Antennas Propag.* **2021**, *69*, 6322–6332. [[CrossRef](#)]
9. Malik, B.T.; Doychinov, V.; Hayajneh, A.M.; Zaidi, S.A.R.; Robertson, I.D.; Somjit, N. Wireless power transfer system for battery-less sensor nodes. *IEEE Access* **2020**, *8*, 95878–95887. [[CrossRef](#)]
10. Lin, W.; Ziolkowski, R.W. Electrically small Huygens antenna-based fully-integrated wireless power transfer and communication system. *IEEE Access* **2019**, *7*, 39762–39769. [[CrossRef](#)]

11. Seo, D.; Varshney, L.R. Information and energy transmission with experimentally sampled harvesting functions. *IEEE Trans. Commun.* **2019**, *67*, 4479–4490. [[CrossRef](#)]
12. Wagih, M.; Hilton, G.S.; Weddell, A.S.; Beeby, S. 2.4 GHz wearable textile antenna/rectenna for simultaneous information and power transfer. In Proceedings of the 2021 15th European Conference on Antennas and Propagation (EuCAP), Dusseldorf, Germany, 22–26 March 2021. [[CrossRef](#)]
13. Lu, P.; Song, C.; Huang, K.M. A two-port multipolarization rectenna with orthogonal hybrid coupler for simultaneous wireless information and power transfer (SWIPT). *IEEE Trans. Antennas Propag.* **2020**, *68*, 6893–6905. [[CrossRef](#)]
14. Zhao, Y.; Hu, J.; Xie, A.; Yang, K.; Wong, K.K. Receive spatial modulation aided simultaneous wireless information and power transfer with finite alphabet. *IEEE Trans. Wirel. Commun.* **2020**, *19*, 8039–8053. [[CrossRef](#)]
15. Sezgin, I.C.; Cisneros, J.-R.P.; Fager, C. Evaluation of simultaneous wireless information and power transfer with distributed antennas. In Proceedings of the 2020 50th European Microwave Conference (EuMC), Utrecht, The Netherlands, 12–14 January 2021; pp. 518–521. [[CrossRef](#)]
16. Song, Z.; Zhang, Z.; Liu, X.; Liu, Y.; Fan, L. Simultaneous cooperative spectrum sensing and wireless power transfer in multi-antenna cognitive radio. *Phys. Commun.* **2018**, *29*, 78–85. [[CrossRef](#)]
17. Clerckx, B.; Huang, K.; Varshney, L.; Ulukus, S.; Alouini, M. Wireless power transfer for future networks: Signal processing machine learning computing and sensing. *IEEE J. Sel. Top. Signal Process.* **2021**, *15*, 1060–1094. [[CrossRef](#)]
18. Gandhiraj, R.; Soman, K. Modern analog and digital communication systems development using GNU Radio with USRP. *Telecommun. Syst.* **2014**, *56*, 367–381. [[CrossRef](#)]
19. Ferdik, M.; Hesche, M.S.; Rack, L.; Saxl, G.; Ussmueller, T. NI PXIe based UHF RFID reader. In Proceedings of the 11th German Microwave Conference (GeMiC), Freiburg, Germany, 12–14 March 2018; pp. 303–306. [[CrossRef](#)]
20. Humphries, J.R.; Kisner, R.A.; Killough, S.M.; Theodore, M.; Polsky, Y. Carbon Fiber Tow Inspection Technique Using Software Defined Radios. *IEEE Sens. Lett.* **2018**, *2*, 6000904. [[CrossRef](#)]
21. Vannucci, G.; Bletsas, A.; Leigh, D. A software-defined radio system for backscatter sensor networks. *IEEE Trans. Wirel. Commun.* **2008**, *7*, 2170–2179. [[CrossRef](#)]
22. Meier, J.; Kelley, R.; Isom, B.M.; Yeary, M.; Palmer, R.D. Leveraging software-defined radio techniques in multichannel digital weather radar receiver design. *IEEE Trans. Instrum. Meas.* **2012**, *61*, 1571–1582. [[CrossRef](#)]
23. Stancombe, A.E.; Bialkowski, K.S.; Abbosh, A.M. Portable microwave head imaging system using software-defined radio and switching network. *IEEE J. Electromagn. RF Microw. Med. Biol.* **2019**, *3*, 284–291. [[CrossRef](#)]
24. Collins, T.F.; Getz, R.; Pu, D.; Wyglinski, A.M. *Software-Defined Radio for Engineers*; Artech House: Norwood, MA, USA, 2018; pp. 289–298.
25. Papoči, P.; Radišić, T.; Muštra, M. Integration of software defined radio on an unmanned aerial vehicle. *Transp. Res. Proc.* **2022**, *64*, 308–315. [[CrossRef](#)]
26. Ni, Z.; Huang, B. Gait-Based Person Identification and Intruder Detection Using mm-Wave Sensing in Multi-Person Scenario. *IEEE Sens. J.* **2022**, *22*, 9713–9723. [[CrossRef](#)]
27. Han, K.; Hong, S. Detection and localization of multiple humans based on curve length of I/Q signal trajectory using MIMO FMCW radar. *IEEE Microw. Wirel. Compon. Lett.* **2021**, *31*, 413–416. [[CrossRef](#)]
28. Zheng, L.; Lops, M.; Eldar, Y.C.; Wang, X. Radar and communication coexistence: An overview: A review of recent methods. *IEEE Signal Process. Mag.* **2019**, *36*, 85–99. [[CrossRef](#)]
29. Kuo, N.-C.; Niknejad, A.M. RF-powered-tag intermodulation uplink with three-tone transmitter for enhanced uplink power. *IEEE J. Radio Freq. Identif.* **2019**, *3*, 56–66. [[CrossRef](#)]
30. Charvat, G.L. *Small and Short-Range Radar Systems*, 1st ed.; CRC Press: Boca Raton, FL, USA, 2014; pp. 281–288.
31. Mercuri, M.; Soh, P.J.; Pandey, G.; Karsmakers, P.; Vandenbosch, G.A.E.; Leroux, P.; Schreurs, D. Analysis of an indoor biomedical radar-based system for health monitoring. *IEEE Trans. Microw. Theory Technol.* **2013**, *61*, 2061–2068. [[CrossRef](#)]
32. Işiker, H.; Özdemir, C. Adaptation of stepped frequency continuous waveform to range-Doppler algorithm for SAR signal processing. *Digit. Signal Process.* **2020**, *106*, 102826. [[CrossRef](#)]
33. Qaragoz, Y.; Pollin, S.; Schreurs, D. Enhanced two-way communication for battery-free wireless sensors: SWIPT with IM3 backscattering. In Proceedings of the 2022 IEEE/MTT-S International Microwave Symposium, Denver, CO, USA, 19–24 June 2022; pp. 48–51. [[CrossRef](#)]